Aeroelastic Analysis of Engine Nacelle Strake Considering Geometric Nonlinear Behavior

N. Manoj

***Abstract*—**The aeroelastic behavior of engine nacelle strake when subjected to unsteady aerodynamic flows is investigated in this paper. Geometric nonlinear characteristics and modal parameters of nacelle strake are studied when it is under dynamic loading condition. Here, an N-S based Finite Volume solver is coupled with Finite Element (FE) based nonlinear structural solver to investigate the nonlinear characteristics of nacelle strake over a range of dynamic pressures at various phases of flight like takeoff, climb, and cruise conditions. The combination of high fidelity models for both aerodynamics and structural dynamics is used to predict the nonlinearities of strake (chine). The methodology adopted for present aeroelastic analysis is partitioned-based time domain coupled CFD and CSD solvers and it is validated by the consideration of experimental and numerical comparison of aeroelastic data for a cropped delta wing model which has a proven record. The present strake geometry is derived from theoretical formulation. The amplitude and frequency obtained from the coupled solver at various dynamic pressures is discussed, which gives a better understanding of its impact on aerodynamic design-sizing of strake.

***Keywords*—**Aeroelasticity, finite volume, geometric nonlinearity, limit cycle oscillations, strake.

I. Introduction

THE aeroelasticity is one of the most important classes of fluid-structure interaction (FSI) problems. It is relevant for aeronautical disciplines. The aeroelastic analysis is interaction among inertial, elastic, and aerodynamic forces [1], [5]. The phenomenon associated to nonlinearity in fluid and structure is known as Limit Cycle Oscillations (LCOs). This phenomenon gives undesirable results in reduction of vehicle performance which leads to structural fatigue. LCOs are associated with nonlinear aerodynamic mechanisms such as vortex induced vibration, shock induced flow separation and shock wave motions [5], [6]. Investigating LCO is challenging due to the inherent non-linear nature of the problem. Even with the presence of accurate methods and wind tunnel test data finding the existence of LCO is difficult owing to the fact that it is unable to distinguish LCO from the onset of flutter occurrence [5]. Hence, it demands the need to develop good non-linear prediction techniques for simulation of LCO.

Computational fluid dynamics (CFD) solver coupling with computational structural dynamics (CSD) solver provides a prediction capability for simulating the complex, nonlinear aerodynamics and structural dynamics associated with LCO phenomena. Investigations using non-linear structural models in computational aeroelasticity have been done by few researchers [2]. The present work investigates the existence of amplitude self-sustaining vibration resulting from the nonlinear interaction between the unsteady aerodynamics and the structural response. LCO problem of the strake is investigated using three dimensional solid elements.

Manoj N. is with the QuEST Global Pvt Ltd, Bangalore, India, (phone: +9180-67091574; e-mail: manoj.nataraj@ quest-global.com).

II. Theory and Methodology

The methodology adopted for the present analysis is the partitioned based coupled CFD and CSD solvers in time domain. This has been validated with other research papers and with experimental test [3], [7], [8].

A. Governing Equation of Fluid Dynamics

Moving or deformable control volume governing equation of a fluid flow in integral form of N-S equation is shown in (1).

$$\frac{\partial}{\partial t}\int_v W dV. + \oint [F - G].dA = \int_v H dV \tag{1}$$

where the vectors W (vector of conservative variables), F (vector of convective fluxes) and G (vector of diffusive fluxes) are defined in (2):

$$W = \begin{Bmatrix} \rho \\ \rho \mathrm{V} \\ \rho \mathrm{E} \end{Bmatrix} \quad F = \begin{Bmatrix} \rho(v - v_g) \\ \rho(v - v_g) \otimes v + \rho I \\ \rho(v - v_g) H + \rho v_g \end{Bmatrix} \quad W = \begin{Bmatrix} 0 \\ T \\ \mathrm{T.v} + \dot{\mathrm{q}}'' \end{Bmatrix} \tag{2}$$

and the vector H contains the body forces and energy sources. Here ρ, v, v_g, E and p are the density, velocity vector, grid velocity vector, total energy per unit mass and pressure of the fluid, respectively. T is the viscous stress tensor and $\dot{q}''$ is the heat flux. Nonlinear set of equations is solved using algebraic multi-grid approach. Dual-time stepping approach is used for unsteady flow simulation. Spatial and temporal discretization schemes used for analysis are listed in Table I.

TABLE I
Spatial and Temporal Discretization Schemes

Terms	Discretization
Temporal term	Implicit, second order
Convective term	Roe's flux difference splitting scheme
Diffusive term	Second-order accurate and upwind scheme
Gradients	Hybrid Gauss -LSQ

B. Governing Equation of CSD

Based on principle of virtual work, the nonlinear differential

equation is written in matrix form as described in (3).

$$[M]\ddot{x} + [C]\dot{x} + [K]x = F(t) \quad (3)$$

where [M], [C], and [K] are the mass, damping and stiffness matrices respectively and F(t) is the applied load vector which are due to pressure and shear stress. $\ddot{x}$, $\dot{x}$, and x are the vector of acceleration, velocity, and displacement respectively. The system of nonlinear differential equations is solved using iterative Newton-Raphson procedure at each time instance and the Hilbert-Hughes-Taylor (HHT) time integration algorithm is used to advance the structural solution forward in time.

C. CFD and CSD Coupling

Fig. 1 explains the coupling process used in aeroelastic analysis. This methodology is adopted in the present work to study the nonlinear characteristics of the nacelle strake.

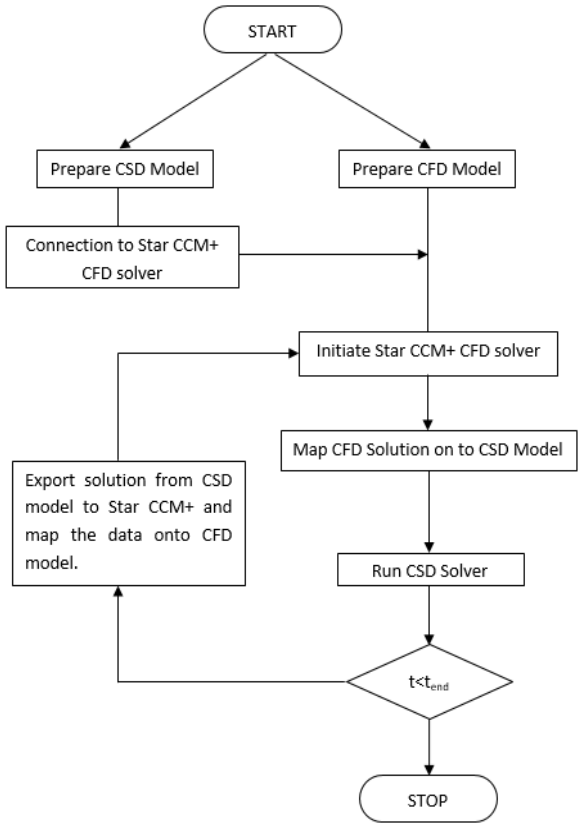

Fig. 1 Simulation using CFD and CSD solvers for analysis

Aerodynamic force acting on the structure is computed by the unsteady CFD solver, whereas the displacements are computed by the nonlinear structural solver. The loosely coupled strategy is adopted in the present work in which the aerodynamic forces are updated on the structure and the aerodynamic mesh are updated using the structural displacements at the end of every physical time step. Compatibility and equilibrium conditions in the fluid-structure interface are achieved without sub-iterations.

III. Computational Setup for Numerical Test

A. Geometric Details

The strake geometry shown in Fig. 2 is defined by (4) which has been taken from the US patent [4] and other research projects.

$$y = HG * \left[1 - \frac{(LG - x)^2}{LG^2}\right] \quad (4)$$

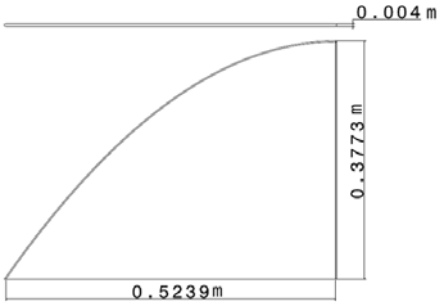

Fig. 2 Geometric details of nacelle strake

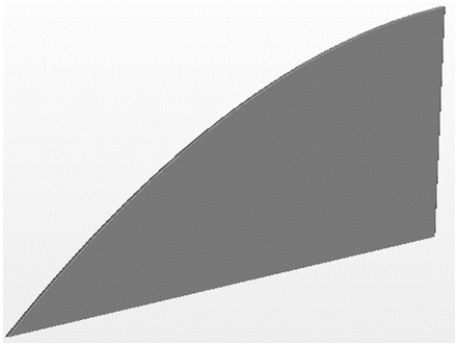

Fig. 3 Isometric view of nacelle strake

The length of the strake is defined keeping in mind that the typical ratio of length of the vortex generator to the length of the nacelle is 10% to 15%, y is the height coordinate of the vortex generator, i.e. strake with a maximum height HG. x is the longitudinal coordinate of the vortex generator with an overall length LG. For case studies, engine diameter and nacelle length is considered as 1.836 m and 5.38m respectively with the fineness ratio of 1.5 [9]. The thickness, height, and length of the model is 0.004 m, 0.3773 m and 0.5239 m, respectively. Analysis is carried out by assuming that strake geometry oriented to the flow field is at zero-degree angle. The thickness distribution is uniform throughout the profile.

B. Computational Data Used for Analysis

The structural dynamic model is created using high order solid element with 7220 nodes. The fluid dynamics model is created using polyhedral cells. The total number of cells in the fluid domain is 940093. The boundary layer is modeled with 10 prism layers with first cell height 0.00001 m and total thickness 0.0001 m. Edges of the strake is refined in order to capture the flow gradients accurately. The computational

meshes used for structural dynamics and aerodynamics calculations are shown in Figs. 3 and 4, respectively. Prism layer mesh near the leading edge of strake is shown in Fig. 5.

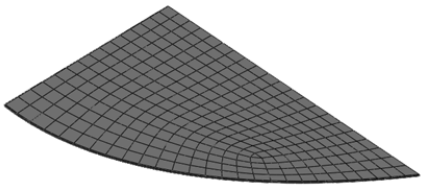

Fig. 4 CSD mesh for strake

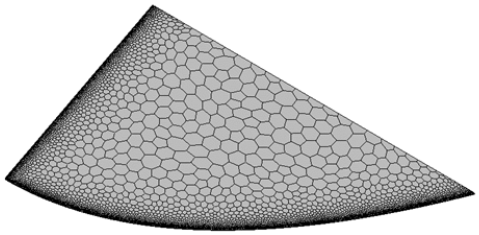

Fig. 5 CFD grid on strake surface

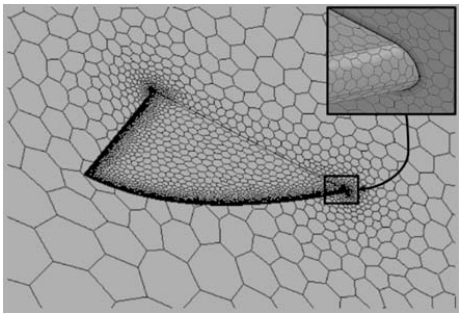

Fig. 6 Mesh of fluid near to strake

C. Flow Parameters and Boundary Conditions.

Considering the typical values of operational Mach number for commercial aircrafts, the flow parameters used for investigation are defined in Table III. Moving mesh boundary method is employed between the interface of fluid and structure mesh. The interface region of solid and fluid mesh is partitioned based approach, and the nodes of structure and fluid at this region are explicitly coupled.

TABLE II
FLOW PARAMETERS FOR ANALYSIS

Sl. no	Flight Path	Altitude (ft.)	Mach number	AOA (deg)
1	Take off and Initial climb	0	0.2-0.3	0 to 6
2	Maximum climb	10000	0.47-0.6	5 to 6
3	Cruise	16000	0.71-0.79	2 to 3

International Standard Atmosphere (ISA) data are used to get the environmental conditions at each stages of flight path.

IV. RESULTS AND DISCUSSION

A. Free Vibrational Analysis.

Free vibrational analysis is carried out to check the existence of rigid modes of a structure, to find the mass participation factor and the structural discrepancies of nacelle strake. Strake is made of aluminum material whose properties are Young's modulus (E) = 70 GPa, density(ρ_s) = 2700 kg/m^3 and Poisson's ratio (v) = 0.3. The nacelle strake is rigidly constrained at its root section in all the degrees of freedom. Table III shows the natural frequency, mode shape, and its corresponding eigenvalues.

TABLE III
MODAL PARAMETERS

Sl. no	Mode Shape	Natural Frequency (Hz)	Eigen value
1	First Bending	29.575	34531.00698
2	First Torsion	87.119	299630.1420
3	First Fore-Aft Bending	162.000	1036071.592
4	Second Torsion	205.87	1673192.333

Mass of the strake is 1.428156 kg and its moments of inertia about center of mass is $I_{xx} = 1.3881*10^{-02}$ m^4, $I_{yy} = 2.3551*10^{-02}$ m^4, $I_{zz} = 3.7429*10^{-02}$ m^4.

The mode shapes corresponding to the first four natural frequencies are also shown in Fig. 7.

(a) Mode1 (29.575 Hz)

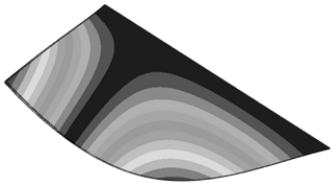

(b) Mode 2 (87.119 Hz)

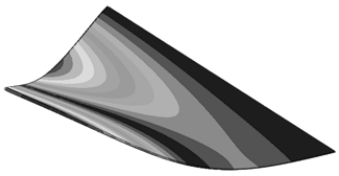

(c) Mode 3 (162 Hz)

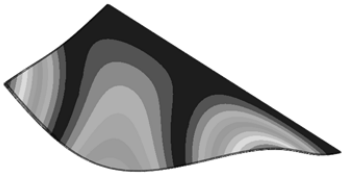

(d) Mode 4 (205.87 Hz)

Fig. 7 First four mode shapes and natural frequencies nacelle strake

B. Case Studies to Predict LCO

Dynamic pressures adopted for investigation of strake are

listed in Table IV.

TABLE IV
FLOW CONDITIONS

Dynamic Pressure (kPa)	Mach Number	Reynolds Number
27.39	0.20	$3.20*10^6$
41.05	0.47	$2.80*10^6$
36.54	0.71	$1.72*10^6$
45.23	0.79	$1.91*10^6$

Initial flow conditions are obtained by a previous converged steady state simulation over an un-deformed nacelle strake configuration. The fluid structure interaction analysis is triggered by a steady state simulation over a strake surface. The conditions chosen for the FSI analysis are free stream Mach number (M_∞) and free stream Reynolds number (Re_∞) as listed in the table. At these conditions, responses of nacelle strake are observed. Courant number of 5 is adopted for CFD algorithm, and the time step used for the simulation is 0.0001 s with 10 inner iterations per physical time step. The turbulence in the flow is modelled using k-omega SST turbulence model. In the present work, it is assumed that there is no structural mass damping in the system. In the previous section, we got to know the modal parameters of strake, keeping this in mind that the investigation of geometric and aerodynamic nonlinearities is proceeded further to predict the LCO behavior in terms of amplitude and frequency on application of unsteady aerodynamic load. From Figs. 8-10, out of phase oscillations between nacelle strake edge motion and the lift coefficient can be observed. The corresponding time history of lift coefficients and amplitudes is presented. The aerodynamic effects are calculated in the fluid mesh over the fluid-structure boundary and in the mesh of FE model of structure. Lift is 180° out of phase with respect to displacement response, acting as a spring like force that always restores the strake to its undeformed configuration. Due to large deformation of nonlinear structural model strake tip vortices are generated at high intensity. The nonlinear mechanism of aerodynamics is the cause of vortex strength over strake edges.

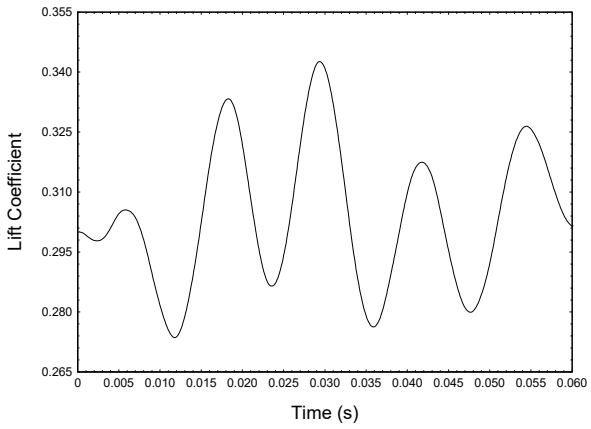

(a) Lift coefficient at q_∞ 27.39kPa

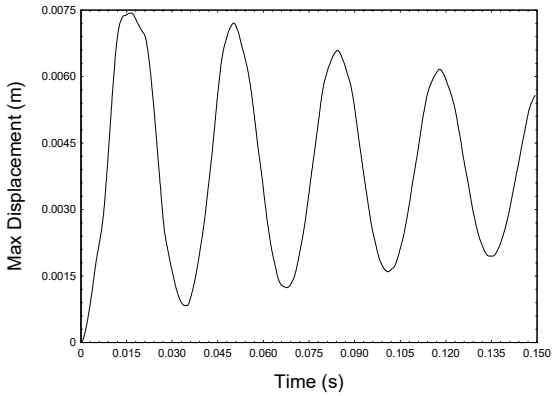

(b) Max displacement at q_∞ 27.39kPa

Fig. 8 Time history of displacement and lift coefficient at M∞ 0.2 of AOA 6 deg

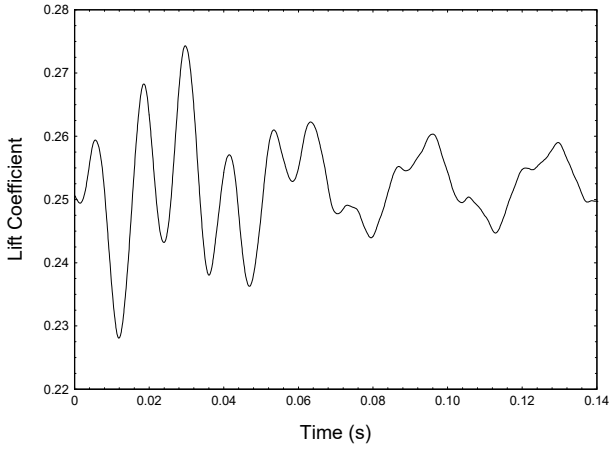

(a) Lift coefficient at q_∞ 41.05 kPa

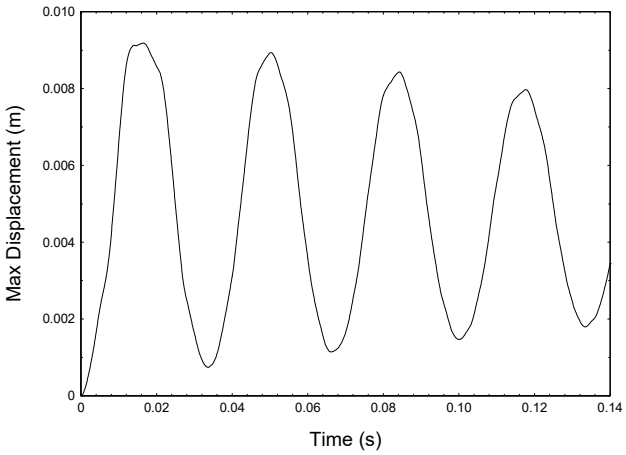

(b) Max displacement at q_∞ 41.05 kPa

Fig. 9 Time history of displacement and lift coefficient at M∞ 0.47 of AOA 5 deg

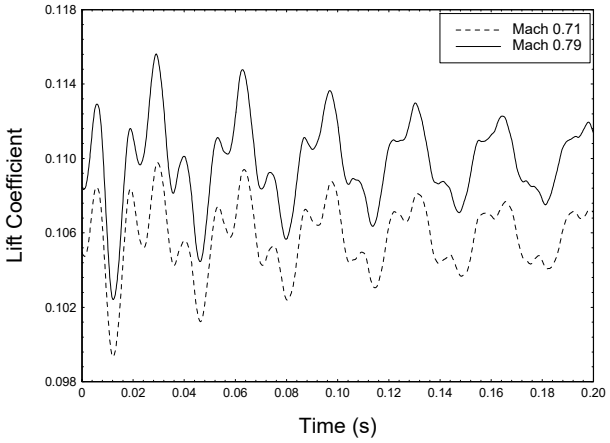

(a) Lift coefficient at q_∞ 36.54 kPa and 45.23kPa

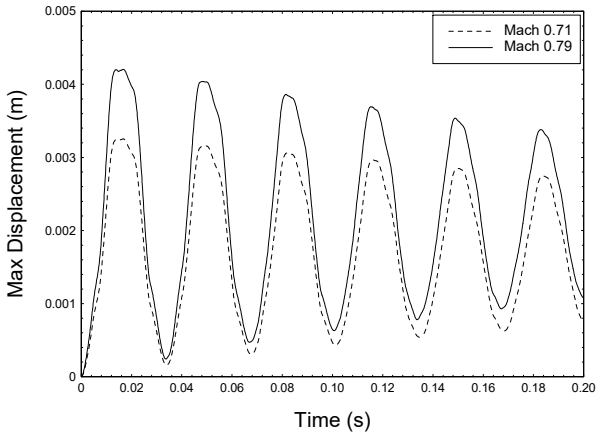

(b) Max displacement at q_∞ 36.54 kPa and 45.23kPa

Fig. 10 Time history of displacement and lift coefficient at AOA 2 deg of q_∞ 36.54 kPa and 45.23 kPa

The strengthened vortex creates normal force which acts at 180° phase. This intensified vortex acts like an aerodynamic spring which ignites the presence of LCO [3]. LCO is due to the presence of the nonlinear mechanism in the aerodynamics.

As the strake deforms, a non-zero local angle of attack is created by the resultant component of the aerodynamic loads. The increase in this angle of attack again results in the production of a vortex at strake tip. Thus, the generation of LCO in the present case is due to the nonlinearity in the aerodynamic sources. It is also observed that, tip vortices are very strong. Thus, the amplitude and oscillations of LCO are primarily caused by the nonlinearity present in the structure. The response and frequencies for various dynamic pressures are listed in Table V.

TABLE V
STRUCTURAL RESPONSES

Dynamic Pressure (kPa)	Amplitude (m)	Frequency (Hz)
27.39	0.00744	26.8
41.05	0.00919	33.1
36.54	0.00325	31.1
45.23	0.00420	29.8

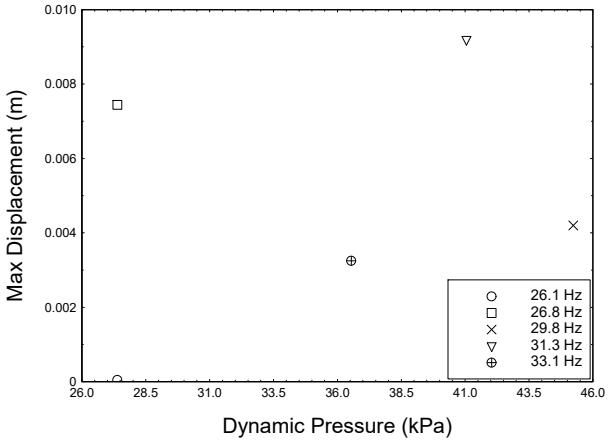

Fig. 11 Comparison of LCO amplitudes at different dynamic pressure

Fig. 11 shows the comparison of LCO amplitudes at different dynamic pressures and it is observed that, at dynamic pressure 41.05 kPa, the amplitude of 0.00919 m is high compared to other phases of flight path. But, vibrational behavior is of 31.3 Hz which leads to bending action of strake. This says that the structure is stable at this condition. There is no contribution of couple mode when structure experiences the unsteady aerodynamic load for a given flow condition.

Fig. 12 shows the frequencies at each dynamic pressure which are listed in Table V.

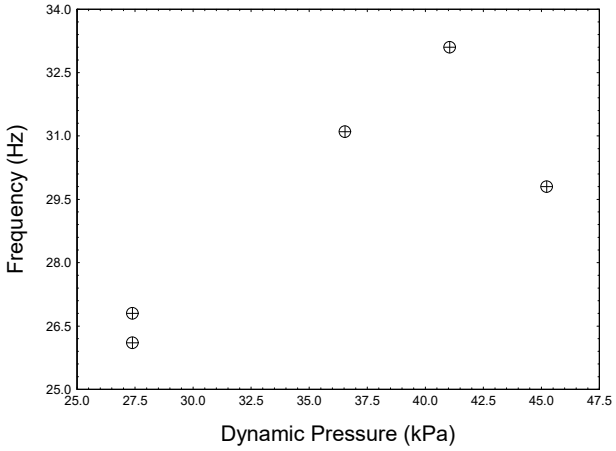

Fig. 12 Comparison of frequencies at different dynamic pressure

V. CONCLUSION REMARKS

In this study, LCO predictions for engine nacelle strake have been successfully conducted considering vortex induced vibration effect. Detailed aeroelastic responses are computed in time domain in order to investigate the aeroelastic characteristics by considering higher end turbulence models.

Investigation done in the present paper shows that the strake has a capability to generate lift and has a significant effect in generating vortices under aeroelastic vibrations. Hence, it gives an essence of consideration of aeroelastic effect for aerodynamic design and sizing of strake.

ACKNOWLEDGMENT

The author would like to thank Sailesh and Geethanjali for their support.

REFERENCES

[1] R. E. Gordnier, Computation of limit cycle oscillations of a delta wing, 43rd AIAA/ASME/ASCE/AHS/ASC Structures, Structural Dynamics, and Materials Conference, 22-25 April 2002, Denver, Colorado, USA.

[2] P. J. Attar and R. E. Gordnier. Aeroelastic prediction of the limit cycle oscillations of a cropped delta wing. Journal of Fluids and Structures, 22(1):45 – 58, 2006.

[3] A Arun Kumar, N. Manoj, Amit Kumar Onkar, M Manjuprasad, Fluid-Structure Interaction analysis of a Cropped Delta Wing, 12th International Conference on Vibration Problems, ICOVP 2015, Procedia Engineering 144 (2016) 1205 – 1212, Elsevier journal.

[4] Michael L. and Henderson, R.B.O (1987) ―Nacelle/wing assembly with vortex control device‖. Patent no. US 4685643. Available at: *www.google.com/patents/US4685643.pdf*.

[5] Raymond E. Gordnier. Computation of limit-cycle oscillations of a delta wing. Journal of Aircraft, 40(6):1206–1208, 2003.

[6] Raymond Gordnier and Reid Melville. Numerical Simulation of Limit-cycle Oscillations of a Cropped Delta Wing Using the Full Navier-Stokes Equations. International Journal of Computational Fluid Dynamics, 14:211–224, 2001.

[7] Jinglong Han Cui Peng. Numerical investigation of the effects of structural geometric and material nonlinearities on limit-cycle oscillation of a cropped delta wing. Journal of Fluids and Structures, 27(4):611 – 622, 2011.

[8] R. E. Gordnier, R. B. Melville, Physical mechanisms for limit-cycle oscillations of a cropped delta wing, 30th AIAA Fluid Dynamics Conference, 28 June - 1 July, 1999, Norfolk, VA.

[9] Ajoy Kumar Kundu, Aircraft design, Cambridge Aerospace series, 2010.